INT. J. REMOTE SENSING, 20 DECEMBER, 2003,
VOL. 24, NO. 24, 5367–5378

Taylor & Francis
Taylor & Francis Group

Calibration of the visible and near-infrared channels of NOAA-11 and -14 AVHRRs by using reflections from molecular atmosphere and stratus cloud

HIRONOBU IWABUCHI

Hydrological Cycle Research Program, Frontier Research System for Global Change, 3173-25 Showa-machi, Kanazawa-ku, Yokohama, Kanagawa 236-0001, Japan; e-mail: hiro-iwabuchi@jamstec.go.jp

(*Received 29 August 2001; in final form 29 January 2003*)

Abstract. A new method to determine the calibration coefficients for visible and near-infrared channels of Advanced Very High Resolution Radiometer (AVHRR) aboard NOAA satellite is presented and applied to NOAA-11 and -14 spacecrafts. The method uses the reflections from clear-sky ocean and stratus clouds. The clear-sky data analysis gives a minimum estimate of the slope coefficient (albedo per count) for a target month by using radiative transfer theory for molecular atmosphere. Cloudy-sky pixels were precisely excluded from that analysis by using multi-spectral data of AVHRR. Neighbouring pixels of cloud were also excluded to avoid three-dimensional radiative effects such as cloud shadow. On the other hand, the optical thickness (at a visible wavelength) of summer stratus clouds was retrieved from nominally calibrated reflectance of respective visible and near-infrared channels. This analysis was performed to adjust the balance between the two-channels' calibration coefficients because if the two channels were correctly calibrated, the cloud optical thickness retrieved from the two channels must be the same. Finally, the calibration coefficients were determined using iteration.

1. Introduction

Advanced Very High Resolution Radiometer (AVHRR) data have been widely used to study the Earth's environment such as ocean, land, vegetation, aerosol and clouds. AVHRR has no on-board calibration device for the visible (channel 1: $\approx$0.58–0.68 μm) and near-infrared (channel 2: $\approx$0.72–1.1 μm) channels, and in-flight calibration is crucial to detect any climatic change at decadal time scale. Since a direct method by aircraft observation is expensive to monitor the long-term calibration, the calibration of the two channels has been performed by indirect methods monitoring the sensor degradation by using semi-permanent reflectance targets such as desert and ice sheet (Kaufman and Holben 1993, Rao and Chen 1995, 1999, Loeb 1997, Tahnk and Coakley 2001). The calibrations presented by several works sometimes show a considerable disagreement. The desert region near the equator has an advantage of a calibration target to be observed throughout a

International Journal of Remote Sensing
ISSN 0143-1161 print/ISSN 1366-5901 online © 2003 Taylor & Francis Ltd
http://www.tandf.co.uk/journals
DOI: 10.1080/0143116031000102403

whole year with a disadvantage of contamination by a large amount of dust aerosols. The ice sheet in the polar region is generally far from the source of pollutant and observed in frequent overpasses by National Oceanic and Atmospheric Administration (NOAA) polar-orbiter satellite, but the observation is restricted to the summer season due to low solar elevation.

Instead of the relative calibration monitoring the sensor degradation, a few absolute calibration methods using molecular scattering data and radiative transfer theory have been presented. Kaufman and Holben (1993) determined NOAA-9 channel 1 calibration by reflection from oceanic clear-sky atmosphere in off-nadir backscattering viewing directions. Higurashi *et al.* (2000) also obtained the calibration for NOAA-11 in 1990 from a comparison of theoretical reflectance of molecular atmosphere against observed minimum count of AVHRR in about $50\,\mathrm{km} \times 50\,\mathrm{km}$ area, and they applied the calibration to characterization of global aerosol properties. In these methods detection of completely cloud-free region and exclusion of cloud shadow are important. These methods can provide an absolute calibration although the uncertainty of the calibration might be large because the clear-sky ocean is relatively dark unlike the desert and ice sheet.

In the present study, a method similar to Kaufman and Holben (1993) is applied to determine the calibration coefficients for the visible and near-infrared channels on the NOAA-11 and -14 spacecrafts. Additionally, the present work uses stratus clouds to reduce the uncertainty and to adjust a balance between the two channels' calibration coefficients. The balance between the two channels is important for climatic study of vegetation (e.g. the Normalized Difference Vegetation Index, NDVI) and aerosol properties.

2. The AVHRR data

The AVHRR albedo (%) for channel i is defined as follows:

$$A_i = \frac{100\pi I_i}{F_{0i}} \tag{1}$$

where I_i is spectral radiance ($\mathrm{W\,m^{-2}\,sr^{-1}\,\mu m^{-1}}$) and F_{0i} is extraterrestrial solar spectral irradiance ($\mathrm{W\,m^{-2}\,\mu m^{-1}}$). The AVHRR albedo is related with observed 10-bit raw count (C_i), as follows:

$$A_i = S_i(\mathrm{C}_i - C_{0,i}) \tag{2}$$

where S_i is slope (%/count) and $C_{0,i}$ deep space count. Following Staylor (1990), the calibration formula for the slope is given by,

$$S_i = m_i \exp(k_i\, d) \tag{3}$$

where d denotes days after launch of spacecraft. Coefficients m_i and k_i are determined from the procedure described in §3. The launch date is 24 September 1988 for NOAA-11 spacecraft and 30 December 1994 for NOAA-14.

Before determination of coefficients m_i and k_i, the deep space counts were determined from night-time observation data. The data of January 1989 and July 1994 for NOAA-11 and of February 1995 and June 1998 for NOAA14 were analysed. For NOAA-11 spacecraft, the deep space count slightly decreases during the lifetime of about 6 years. The formulae for NOAA-11 channels 1 and 2 are

given by,

$$C_{0,1} = 40.02(1 - 0.40 \times 10^{-5}\, d) \tag{4a}$$

$$C_{0,2} = 40.03(1 - 0.66 \times 10^{-5}\, d) \tag{4b}$$

respectively. For NOAA-14 spacecraft, time variation in the deep space count was almost absent, and the determined formula is as follows:

$$C_{0,1} = C_{0,2} = 41.0 \tag{5}$$

The AVHRR data used in the present work were originally processed from High Resolution Picture Transmission (HRPT) data that had been collected in Sendai, Japan since 1980s (Kawamura *et al.* 1993a). The target region for the calibration is the north-western Pacific Ocean and the seas of Japan and Okhotsk: 15–45° N and 120–165° E for the clear-sky analysis and 35–55° N and 140–165° E for stratus cloud analysis. Data over a period from 1988 to 1994 for NOAA-11 and 1995–1999 for NOAA-14 were used. The data were sampled in 1.1 km spatial resolution with geometrical correction. For infrared channels (channel 3: ≈3.5–4.0 μm; channel 4: ≈10.3–11.3 μm; and channel 5: ≈11.5–12.5 μm), the nonlinear radiometric correction was applied (Kawamura *et al.* 1993b).

3. Methodology and procedure

The absolute calibration process for S_i consists of analyses of clear-sky data over the ocean and that of cloudy sky. The clear-sky analysis is similar to Kaufman and Holben (1993). Figure 1 shows theoretical reflectance for molecular atmosphere against corresponding observed AVHRR count averaged over square region of four-pixel width, for clear-sky regions over the ocean. The observed count would increase with aerosol amount, so that the leftmost (lowest) count is associated with the smallest amount of aerosols during the observation period (a month). For each plot, the drawn line connects two points of the deep-space point (count of about 40–41) and the leftmost count datum. The gradient of fitted line gives a minimum estimate of S_i; for smaller amount of aerosol, this estimate exhibits a larger value. The estimations of the minimum S_i were performed monthly. Details of radiative transfer computation and procedure for data processing are given below.

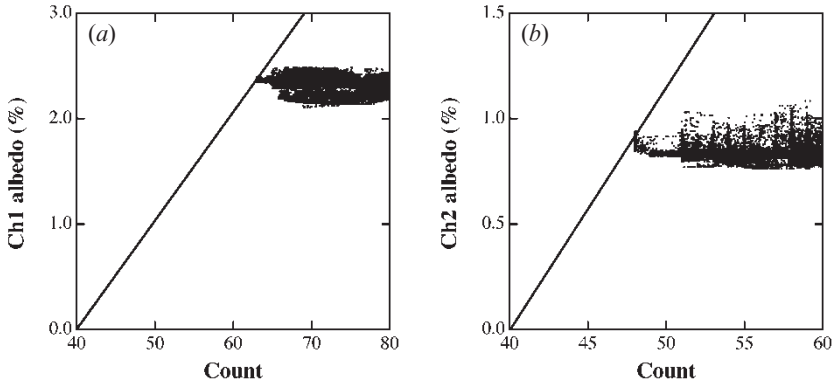

Figure 1. Theoretical albedo for molecular atmosphere against the observed AVHRR count of clear-sky pixels: (*a*) channel 1, (*b*) channel 2.

The theoretical reflectance for the molecular atmosphere over the seas is computed by look-up table (LUT) method. The LUT was made by radiative transfer computation with a code of Nakajima and Tanaka (1986, 1988), in which the discrete ordinate and adding methods are used. The gaseous absorption by ozone, water vapour, and other possible gases is incorporated using the k-distribution model of LOWTRAN-7 (Kneizys *et al.* 1988). A rough ocean model of Nakajima and Tanaka (1983) is also used, in which effect of wind velocity on the reflectance of ocean surface is included. The LUT is made for a grid system of the solar and viewing zenith angles, relative azimuth angle, wind velocity and water vapour, as summarized in table 1. The theoretical reflectance is interpolated from the look-up table for an angular geometry, with a correction for distance between the sun and the earth. The data of wind velocity, water vapour, and ozone are provided from climatic data for respective months and sub-regions of about 1000 km width. The solar and viewing zenith angles are restricted to less than 60° and 35°, respectively, and the geometry near the sun glint is excluded by the cone angle ($>50°$) around the mirror-reflecting direction of the Sun.

Clouds should be excluded from the clear-sky analysis. For that purpose, pixels with channel-4 brightness temperature less than 280 K were excluded. Thin cirrus clouds and warm clouds were detected by larger difference in temperature between channels 3 and 4 than 4 K or between channels 4 and 5 than 2 K. The channel 1 albedo was nominally calibrated with the equations of Rao and Chen (1995, 1999) in the cloud screening process, and a bright pixel with larger albedo than theoretical value for aerosol optical thickness of 1.5 was excluded. To detect thin small-scale broken clouds and cloud edges, the standard deviation of channel 1 reflection function (albedo normalized by cosine of solar zenith angle (θ_0), i.e. $A_i/\cos\theta_0$) was calculated for each 4×4 pixel area. Data with standard deviation larger than 0.3% were excluded. In addition, neighbouring pixels of cloud were also excluded because cloud shadow is a major source of error to estimate the minimum S_i. Figure 2 shows horizontal distribution of the reflection function near cloud, which was calculated with a three-dimensional Monte Carlo radiative transfer model of Iwabuchi and Hayasaka (2002). It is evident that there are shadow and darkening region near the shadow. These regions are so dark that it cannot be explained by radiative transfer theory for plane-parallel atmosphere. If these dark pixels are included in the estimation of the minimum S_i, the estimate is unrealistically large. In the present study, a distance (km) from cloudy pixel to be excluded was given by $D=4.4[1+6\,(1-\cos\theta_0)]$. The distance is 4.4 km for $\theta_0=0°$ and 17.6 km for $\theta_0=60°$. This criterion is robust enough to avoid shadow of high cloud and darkening near

Table 1. Grid parameters for the look-up table for molecular atmosphere reflectance: θ_0, solar zenith angle; θ, viewing zenith angle.

Parameter	Min–Max (spacing)	No. of grids
$\cos\theta_0$	0.34–1 (0.03)	23
$\cos\theta$	0.7–1 (0.02)	16
Relative azimuth angle (°)	0–180 (10)	19
Water vapour path ($g\,cm^{-2}$)	0–5 (1)	6
Wind velocity ($m\,s^{-1}$)	5–12 (1)	8

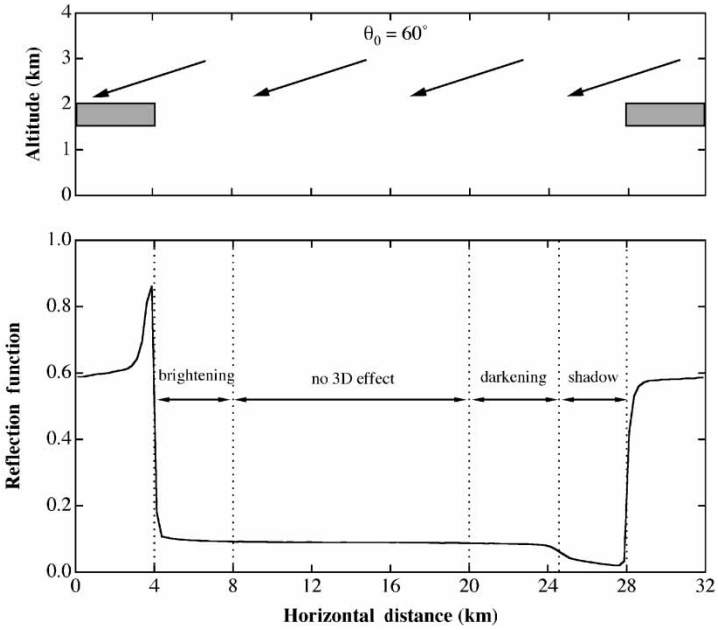

Figure 2. Visible reflection function of clear-sky pixels near cloud, computed by Monte Carlo three-dimensional radiative transfer simulation. Cloud optical thickness is 20, aerosol optical thickness is 0.3, and Lambertian surface with reflectance of 0.06 is assumed. Results are shown for nadir view ($\cos\theta > 0.95$).

the shadow. Only 4×4 pixel area that is completely covered by clear sky without the cloud-neighbour pixel was used for the clear-sky data analysis. The fraction of clear-sky data used for determination of the minimum S_i was about 5%, on average, of all available data.

The cloudy-sky data analysis is performed to obtain the consistency of calibrations of channels 1 and 2. The cloud optical thickness at 0.5 μm wavelength was retrieved from nominally calibrated reflectance of two respective channels. The retrieved values from the two channels must be the same if the sensor calibrations are correct. If the optical thickness retrieved from channel 1 is larger than that of channel 2, then S_1 is too large or S_2 is too small. Oceanic summer stratus clouds frequently appear in the northern Pacific Ocean and the sea of Okhotsk. Their coverage is high and they are horizontally homogeneous, compared with other types of cloud. Averaged cloud optical thickness over 3 months, June, July and August, was calculated. A LUT was made for varying solar and viewing zenith angles, relative azimuth angle, cloud optical thickness, and water vapour path, as summarized in table 2. The aerosol optical thickness of 0.1 at 0.5 μm wavelength, effective droplet radius of 12 μm for cloud (Han *et al.* 1994), and surface wind velocity of 6 m s^{-1} were assumed. The solar and viewing zenith angles are restricted to less than 60° and 40°, respectively, and sun glint geometry is avoided by the cone angle ($>25°$) around the mirror-reflection direction of the Sun. To extract water-phase cloud, two criteria were applied: brightness temperature of channel 4 must be higher than 273 K to exclude cold clouds, and brightness temperature differences between channels 4 and 5 must be less than 2 K to exclude thin cirrus clouds.

Table 2. Grid parameters of the look-up table for cloudy atmosphere reflectance: τ, optical thickness; θ_0, solar zenith angle; θ, viewing zenith angle.

Parameter	Min–Max (spacing)	No. of grids
$\log_2\tau$	0–7 (0.5)	15
$\cos\theta_0$	0.49–0.95 (0.0354)	14
$\cos\theta$	0.75–1 (0.0192)	14
Relative azimuth angle (°)	0–180 (10)	19
Water vapour path ($g\,cm^{-2}$)	2–4 (1)	3

The calibration coefficients m_i and k_i in equation (3) were determined from the following procedure. First, initial estimates of the coefficients were made from time series of the monthly minimum S_i that was obtained from the clear-sky data analysis as described above. This can be ascribed to a principle that the true value for S_i should be larger than or equal to the minimum because the minimum is associated with the smallest amount of aerosol during a month. A fitted line to the time series should be along the upper envelope of the monthly minima of S_i. Because of a large amount of used data, we can sometimes obtain S_i estimates for case of almost absent aerosol, which could be observed for dry day and just after precipitation. The initial estimates may be rather rough. Next, however, we performed an iterative procedure by using additional cloudy-sky data. Three tests were applied as shown in figure 3:

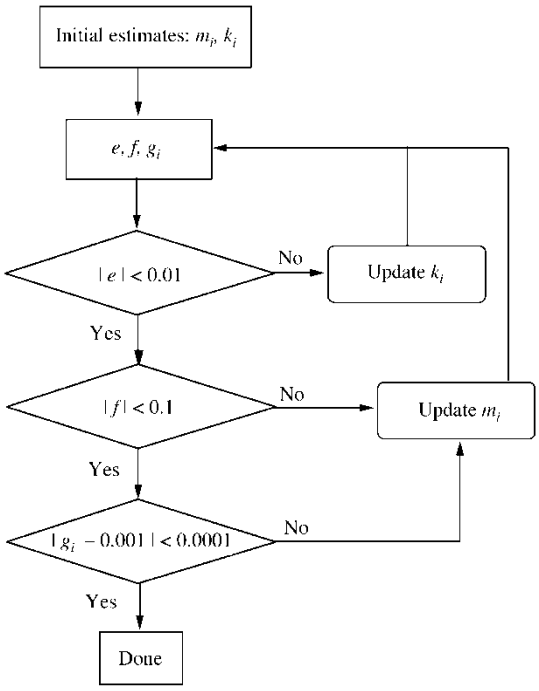

Figure 3. Flow chart of iterative determination of calibration coefficients k_i and m_i. See text for notations.

1. The gradient (T_i per year) of fitted linear line to year-to-year time series of the summer-season averages ($\langle\tau_i\rangle$) of cloud optical thickness retrieved is computed for each channel. The gradients T_1 and T_2 should be almost the same for the consistency between the two-channel calibrations. If $e>0.01$, where $e=T_1-T_2$, then the coefficient k_1 is updated to decrease and k_2 increase. If $e<-0.01$, then the opposite updates are applied.
2. Average over spacecraft lifetime is computed for difference in $\langle\tau_i\rangle$ between the two channels: $f=\overline{\langle\tau_1\rangle-\langle\tau_2\rangle}$. The absolute value of f should be small enough to proceed to the next step. If $f>0.1$, then m_1 is updated to decrease and m_2 increase. If $f<-0.1$, then opposite updates are applied.
3. Average deviation (g_i) of the minimum S_i estimates larger than the fitted curve of equation (3) was calculated. This should be nearly equal to 0.001 to proceed. If $|g_i-0.001|>0.0001$, then m_i is updated. The factor of 0.001 is ascribed to uncertainty in the estimates of minimum S_i due to measurement noise, ocean reflectance, fluctuations in water vapour and ozone.

The iteration finishes when a set of coefficients k_i and m_i clears the three tests. Note that all the updates in the above process are small enough for the parameters e, f, and g_i to converge.

4. Results

Figures 4 and 5 show time series of the monthly minimum estimate of S_i determined by clear-sky analyses for NOAA-11 and -14 spacecrafts, respectively. The Pinatubo effect is clear after June 1991 ($d=1000$ for NOAA-11). The minimum S_i is small after the eruption of Mount Pinatubo because the observed count for clear sky is large due to large amount of background stratospheric aerosol provided by the eruption. The local solar time of afternoon orbit satellites (e.g. NOAA-11 and -14) gradually shifts to late afternoon during lifetime in orbit. For instance, the local solar time for NOAA-11 spacecraft is about 13:30 in November 1988 and 17:00 in September 1994. For more than 1500 days after launch, wintertime data were not analysed because the solar elevation is too low. The minimum S_i varies seasonally with variation of aerosols. As a general tendency, the estimate is large in winter and small in spring. The thick lines in the figures denote the calibration equations determined in the present work. The calibration formulae are written as follows:

NOAA-11:

$$S_1=0.104\ \exp(0.45\times10^{-4}\,d) \tag{6a}$$

$$S_2=0.112\ \exp(0.30\times10^{-4}\,d) \tag{6b}$$

NOAA-14:

$$S_1=0.118\ \exp(0.65\times10^{-4}\,d) \tag{7a}$$

$$S_2=0.1485\ \exp(0.22\times10^{-4}\,d) \tag{7b}$$

Two years since June 1991 with residual effect of Pinatubo eruption is ignored for the determination of these calibration formulae. It is noted that the monthly minimum value of the slope coefficient contains uncertainty due to varying water vapour, ozone and wind velocity.

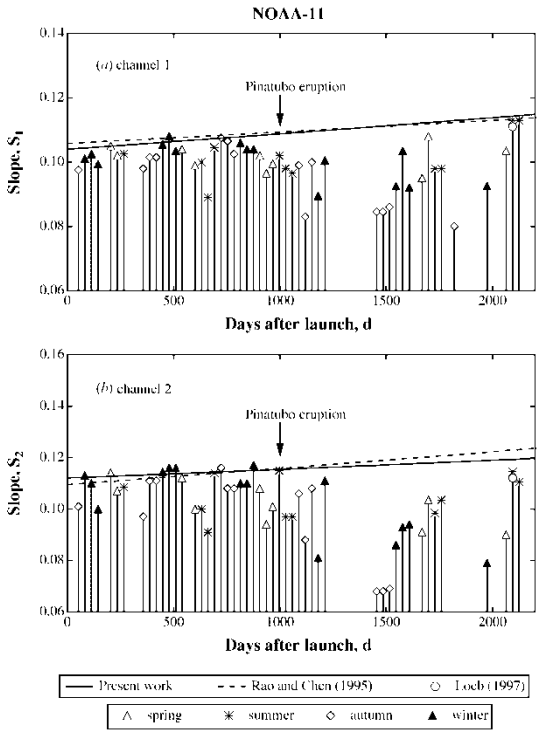

Figure 4. Time series of monthly minimum of the slope coefficient (S_i) for NOAA-11 AVHRR (*a*) channel 1 and (*b*) 2. The calibration results for the present and earlier works are also shown.

The calibrations presented by Rao and Chen (1995, 1999), Tahnk and Coakley (2001) and Loeb (1997) are also plotted in figures 4 and 5. For NOAA-11, the present result of channel 1 is almost the same as Rao and Chen (1995), who used Libyan Desert as a calibration target, and the difference is less than 1.5% throughout the lifetime of the satellite. For channel 2, the increasing rate (k_i) of the slope in the present work is smaller than Rao and Chen (1995). The difference in S_2 reaches 4% at the end of the lifetime of the satellite. For NOAA-14, the increasing rates (k_i) are considerably smaller than Rao and Chen (1999) for both the two channels and close to Tahnk and Coakley (2001) for channel 2, who used ice sheet of Antarctica. The calibrations of the two channels are almost the same as Rao and Chen (1999) at the middle of the satellite lifetime, while the difference reaches about 7% for channel 1 and 10% for channel 2 at the beginning of the satellite lifetime. The present calibration for channel 2 is almost the same as Tahnk and Coakley (2001) throughout the lifetime. That is also true for channel 1 for the 3 years after launch. A possible reason for large rate of k_i in Rao and Chen (1999) might be ascribed to several-year scale variation in dust aerosol amount over the Libyan Desert.

Figure 6 shows time series of average optical thickness of summer stratus clouds over the north-western Pacific Ocean and the sea of Okhotsk, and figure 7 shows frequency distributions of the optical thickness. The average optical thickness is

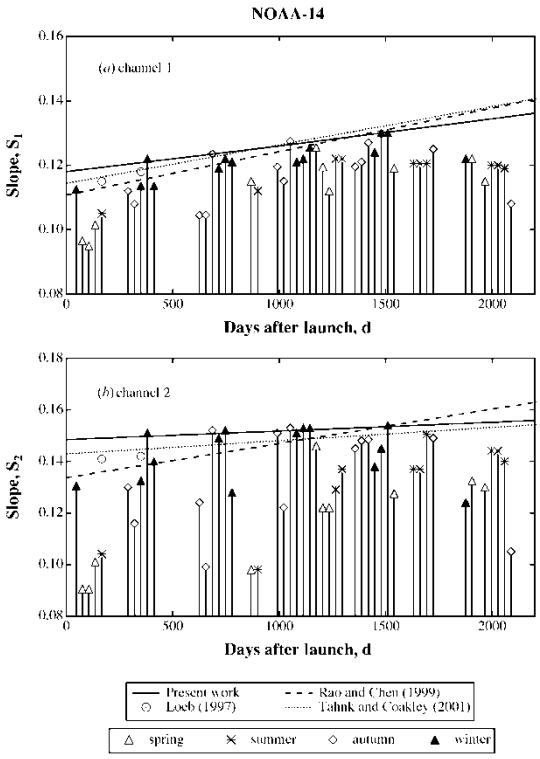

Figure 5. Same as figure 4, but for NOAA-14.

about t 9–11. Retrieved optical thickness in the present work is consistent between the two channels (channels 1 and 2) and between the two spacecrafts (NOAA-11 and -14). Differences between the two channels can be explained by varying water vapour and effective droplet radius mainly. Sensitivity analysis by radiative transfer calculation showed that the uncertainty in retrieved optical thickness is estimated at about 0.2 for channel 1 and 0.3 for channel 2. Results using calibration of Rao and Chen (1995, 1999) and Tahnk and Coakley (2001) are also shown in figure 6 and suggest inconsistency between the two channels.

Figure 8 shows the retrieved optical thickness of horizontally homogeneous stratus cloud with a cloud inhomogeneity test. Horizontally inhomogeneous clouds were excluded from this analysis by using an inhomogeneity parameter, the standard deviation of 10-base logarithm of the optical thickness. A threshold for the inhomogeneity parameter was set at 0.05. It is shown that no gap appears between the results for NOAA-11 and -14 spacecrafts. The optical thickness of homogeneous cloud of the present target region does not vary largely throughout the 11 years. On the other hand, cloud optical thickness without the inhomogeneity test increases in the satellite lifetime with increasing solar zenith angle, especially near the end of the lifetime (figure 6). This is not ascribed to a natural variation but to cloud inhomogeneity, which introduces a bias in retrieved optical thickness depending on the solar elevation since inhomogeneous cloud with bumpy cloud top reflects more than homogeneous flat cloud does (Loeb and Davies 1996, Iwabuchi

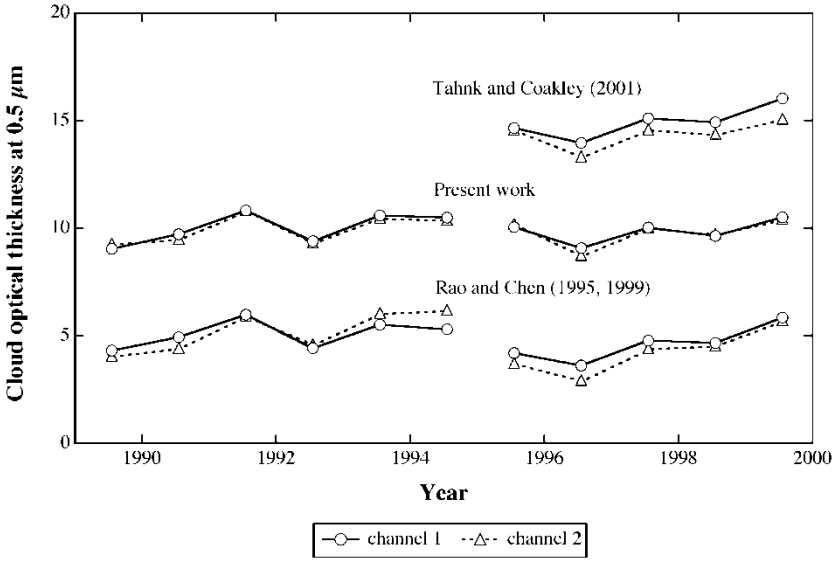

Figure 6. Time series of average optical thickness, at 0.5 μm wavelength, of summer stratus clouds over the north-western Pacific Ocean and the sea of Okhotsk. The optical thickness was retrieved from respective channels of 1 and 2, using calibrations by the present and earlier works. Results of Rao and Chen (1995, 1999) are shifted by -5 and Tahnk and Coakley (2001) by $+5$.

and Hayasaka 2000). The results in figure 8 suggests a possibility to test relative calibration of sensor by monitoring homogeneous stratus clouds.

5. Conclusion

In the present study, a new calibration method for the visible and near-infrared channels of AVHRR has been presented and applied to NOAA-11 and -14 spacecrafts. The method uses the reflections from clear-sky ocean and stratus clouds. In the clear-sky analysis, the cloud shadow and darkening region near the shadow were excluded. The cloudy-sky analysis was used to adjust the balance between the two channels' calibrations because if the two channels are correctly calibrated the cloud optical thickness (at a visible wavelength) retrieved from the two channels must be the same. The balance between the two channels is important for climatic study of vegetation and aerosol properties. The slope coefficients determined in the present work were almost the same as those in Rao and Chen (1995) for NOAA-11 but showed considerably lower rate of sensor degradation than Rao and Chen (1999) for NOAA-14.

Although we selected the north-eastern Asian seas as a target region, other geographical regions may be better for the clear-sky analysis with smaller amount of aerosol (e.g. in the Southern Hemisphere). If data for such clean regions are available, the calibration using clear-sky ocean would be more efficient than demonstrated in the present study. In addition, stratus cloud decks are common with high coverage over the ocean (e.g. summer stratus clouds in the north Pacific Ocean). As a conclusion, it is recommended that clear-sky ocean and stratus cloud decks are included in targets to monitor the sensor calibration.

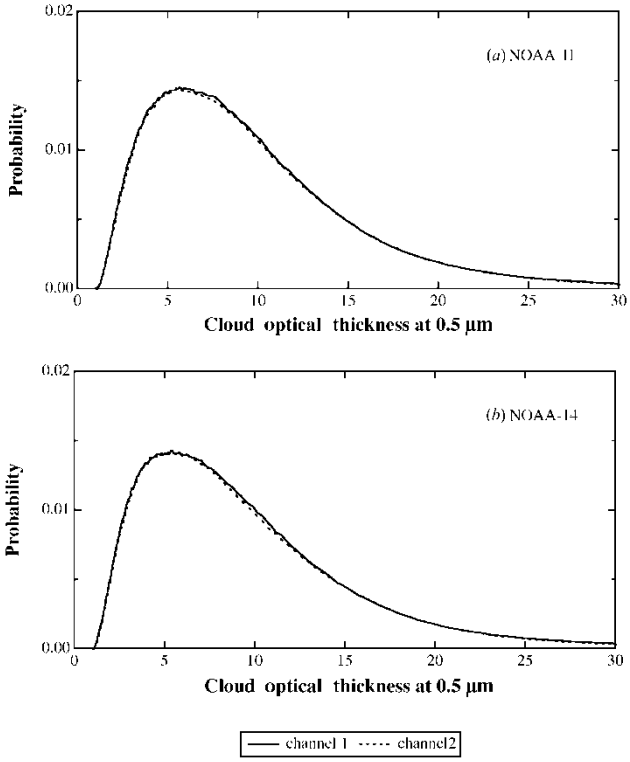

Figure 7. Frequency distributions of retrieved optical thickness for (*a*) NOAA-11 and (*b*) NOAA-14 spacecraft.

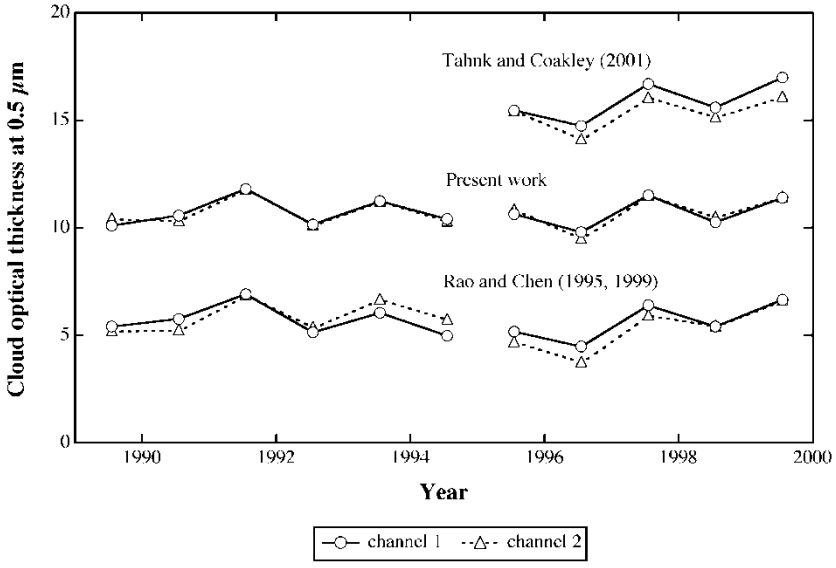

Figure 8. Same as figure 6, but for horizontally homogeneous stratus clouds. Horizontally inhomogeneous clouds were excluded from this analysis by using an inhomogeneity parameter, standard deviation of 10-base logarithm of the optical thickness (>0.05).

Acknowledgment

The author is grateful to Professor H. Kawamura of the Centre for Atmospheric and Oceanic Studies (CAOS), Tohoku University, Japan and Professor J. Kudoh of the Center for Northeast Asian Studies (CNEAS), Tohoku University for providing processed AVHRR data. Processing of AVHRR data by Akira Sobajima of CAOS and Kazuma Hosoi of CNEAS are also acknowledged.

References

HAN, Q., ROSSOW, W. B., and LACIS, A. A., 1994, Near-global survey of effective droplet radii in liquid water clouds using ISCCP data. *Journal of Climate*, **7**, 465–497.

HIGURASHI, A., NAKAJIMA, T., HOLBEN, B. N., SMIRNOV, A., FROUIN, R., and CHATENET, B., 2000, A study of global aerosol optical climatology with two-channel AVHRR remote sensing. *Journal of Climate*, **13**, 2011–2027.

IWABUCHI, H., and HAYASAKA, T., 2002, Effects of cloud horizontal inhomogeneity on the optical thickness retrieved from moderate-resolution satellite data. *Journal of the Atmospheric Sciences*, **59**, 2227–2242.

KAWAMURA, H., KIZU, S., SAKAIDA, F., and TOBA, Y., 1993a, The NOAA-HRPT data receiving system in the Center for Atmospheric and Oceanic Studies in the Tohoku University. *Tohoku Geophysical Journal (Science Report of Tohoku University, Series 5)*, **34**, 89–102.

KAWAMURA, H., SAKAIDA, F., and KIZU, S., 1993b, The AVHRR data processing system in the Center for Atmospheric and Oceanic Studies in the Tohoku University. *Tohoku Geophysical Journal (Science Report of Tohoku University, Series 5)*, **34**, 103–114.

KAUFMAN, Y. J., and HOLBEN, B. N., 1993, Calibration of the AVHRR visible and near-IR bands by atmospheric scattering, ocean glint and desert reflection. *International Journal of Remote Sensing*, **14**, 21–52.

KNEIZYS, F. X., SHETTLE, E. P., ABREU, L. W., CHETWYND, J. H., ANDERSON, G. P., GALLERY, W. O., SELBY, J. E. A., and CLOUGH, S. A., 1988, *Users Guide to LOWTRAN 7.* Report AFGL-TR-88–0177, 137 pp.

LOEB, N. G., 1997, In-flight calibration of NOAA AVHRR visible and near-IR bands over Greenland and Antarctica. *International Journal of Remote Sensing*, **18**, 477–490.

LOEB, N. G., and DAVIES, R., 1996, Observational evidence of plane parallel model biases: apparent dependence of cloud optical depth on solar zenith angle. *Journal of Geophysical Research*, **101**, 1621–1634.

NAKAJIMA, T., and TANAKA, M., 1983, Effect of wind-generated waves on the transfer of solar radiation in the atmosphere–ocean system. *Journal of Quantitative Spectroscopy & Radiative Transfer*, **29**, 521–537.

NAKAJIMA, T., and TANAKA, M., 1986, Matrix formulations for the transfer of solar radiation in a plane-parallel scattering atmosphere. *Journal of Quantitative Spectroscopy & Radiative Transfer*, **35**, 13–21.

NAKAJIMA, T., and TANAKA, M., 1988, Algorithms for radiative intensity calculations in moderately thick atmospheres using a truncation approximation. *Journal of Quantitative Spectroscopy & Radiative Transfer*, **40**, 51–69.

RAO, C. R. N., and CHEN, J., 1995, Inter-satellite calibration linkages for the visible and near-infrared channels of the advanced very high resolution radiometer on the NOAA-7, -9, and -11 spacecraft. *International Journal of Remote Sensing*, **16**, 1931–1942.

RAO, C. R. N., and CHEN, J., 1999, Revised post-launch calibration of the visible and near-infrared channels of the advanced very high resolution radiometer (AVHRR) on the NOAA-14 spacecraft. *International Journal of Remote Sensing*, **20**, 3485–3491.

STAYLOR, W. F., 1990, Degradation rates of the AVHRR visible channel for the NOAA 6, 7, and 9 spacecraft. *Journal of Atmospheric and Oceanic Technology*, **7**, 411–423.

TAHNK, W. R., and COAKLEY, J. A, JR., 2001, Improved calibration coefficients for NOAA-14 AVHRR visible and near-infrared channels. *International Journal of Remote Sensing*, **22**, 1269–1283.